Inorganic Chemistry

pubs.acs.org/IC

Forum Article

$[Ag_9(1,2\text{-BDT})_6]^{3-}$: How Square-Pyramidal Building Blocks Self-Assemble into the Smallest Silver Nanocluster

Badriah J. Alamer, Megalamane S. Bootharaju, Sergey M. Kozlov, Zhen Cao, Aleksander Shkurenko, Saidkhodzha Nematulloev, Partha Maity, Omar F. Mohammed, Mohamed Eddaoudi, Luigi Cavallo, Jean-Marie Basset, and Osman M. Bakr*

Cite This: *Inorg. Chem.* 2021, 60, 4306–4312

Read Online

ACCESS | Metrics & More | Article Recommendations | Supporting Information

ABSTRACT: The emerging promise of few-atom metal catalysts has driven the need for developing metal nanoclusters (NCs) with ultrasmall core size. However, the preparation of metal NCs with single-digit metallic atoms and atomic precision is a major challenge for materials chemists, particularly for Ag, where the structure of such NCs remains unknown. In this study, we developed a shape-controlled synthesis strategy based on an isomeric dithiol ligand to yield the smallest crystallized Ag NC to date: $[Ag_9(1,2\text{-BDT})_6]^{3-}$ (1,2-BDT = 1,2-benzenedithiolate). The NC's crystal structure reveals the self-assembly of two Ag square pyramids through preferential pyramidal vertex sharing of a single metallic Ag atom, while all other Ag atoms are incorporated in a motif with thiolate ligands, resulting in an elongated body-centered Ag_9 skeleton. Steric hindrance and arrangement of the dithiolated ligands on the surface favor the formation of an anisotropic shape. Time-dependent density functional theory based calculations reproduce the experimental optical absorption features and identify the molecular orbitals responsible for the electronic transitions. Our findings will open new avenues for the design of novel single-digit metal NCs with directional self-assembled building blocks.

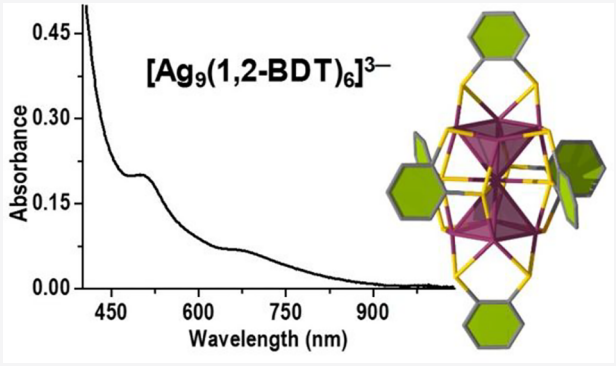

INTRODUCTION

Investigation of the synthesis and chemistry of noble-metal nanoclusters (NCs), such as Au and Ag, is extensively growing[1−4] and has set the scene for establishing these materials as promising candidates for an expansive range of applications, including medical therapy,[5] drug delivery,[6] sensing,[7,8] and catalysis.[9−11] NCs are particularly desirable for catalysis because of their high catalytic activity and/or selectivity.[12,13] The major conceptual driver for NC utilization in catalysis is based on maximization of the per-atom reaction efficiency through control of the metal particle's size from the nanometer to subnanometer scale and ultimately to a few single atoms.[14,15] Therefore, NCs exhibit a range of unique and often unexpected properties compared to larger nanoparticles and bulk materials. This distinct behavior is due to a variety of factors, including the quantum size effect, geometric shell closing,[16] and low-coordination environment. Recently, considerable efforts were devoted to the synthesis of atomically precise clusters with well-defined, stable, and tunable compositions,[17,18] with the aim of achieving a rigorous basis for understanding the correlation between the NCs' structures and their properties.

Metal NCs with single-digit metallic atoms present the highest potential for catalytic activity and also the closest bridge to atomic-level behavior. Metal NCs with fewer than 10 metal atoms not only are good candidates for catalysis but also serve as ideal models to explore the relationship between the metal interface, protecting ligands, and their catalytic activities.[15] Unfortunately, the fabrication of stable thiolated NCs of Ag, Au, or Cu, with less than 10 atoms, remains difficult to achieve compared to the easier preparation of larger particles.

To date, most of the well-known examples of monolayer-protected Ag NCs are large and quasi-spherical,[19−25] whereas only a few limited NCs displayed anisotropic geometries.[26−29] However, there are studies regarding smaller species ($n < 10$) that differ in the size and composition with various types of capping ligands, namely, $Ag_7(DMSA)_4$,[30] $Ag_8(H_2MSA)_8$,[31] and $Ag_9(H_2MSA)_7$.[32] These limited numbers of species—nominally assigned as NCs based on their compositions and molecular weights have unknown crystal structures. Further-

Received: February 4, 2021
Published: March 17, 2021

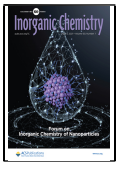

more, stability remains the main obstacle in the synthesis and crystallization of Ag NCs with fewer than 10 metal atoms because Ag is prone to oxidation and is sensitive to light. In Au, while there are several phosphine-protected NCs with few metal atoms,[33,34] the relatively large thiolate Au cluster $Au_{15}(SR)_{13}$[35] is considered to be the smallest NC so far. Only in Cu has the synthesis and crystallization of clusters with fewer than 10 metal atoms been achieved in the form of $Cu_6(SR)_6$. However, it can be easily oxidized upon exposure to air.[36] These observations inspired us to investigate chemical approaches in order to synthesize stable small silver NCs because no sizes between the $[Ag^I(SR)]$ complexes and $[Ag_n(SR)_m]$ ($10 > n > m$) have been crystallized and structurally solved. In this work, we employed the 1,2-benzenedithiolate (1,2-BDT) ligand to synthesize a Ag NC, $[Ag_9(1,2\text{-BDT})_6]^{3-}$. The crystal structure comprises a Ag_9 metal skeleton formed by the self-assembly of two Ag square pyramids through preferential pyramidal vertex sharing. The optical properties are studied in detail using density functional theory (DFT) calculations.

RESULTS AND DISCUSSION

In the majority of NC syntheses, the size, structure, and properties are controlled by the protecting ligands.[37−40] We reasoned that using a small-footprint bidentate thiol such as 1,2-BDT plays an important role in controlling the size of the NC. The steric hindrance between the two adjacent thiolate groups via S lone-pair electron repulsions and the short distance between S binding sites could terminate the growth of a smaller size cluster. In addition to the ligand structure, other reaction conditions, such as the reducing agent and temperature, are also known to influence the NC size.[41] Considering these facts, our synthesis of $[Ag_9(1,2\text{-BDT})_6]$-$(TOA)_3$ NCs (Figure S1) involves the chemical reduction of silver thiolates [Ag-(1,2-BDT)] in mixed solvents of methanol and dichloromethane (DCM) by an aqueous sodium borohydride ($NaBH_4$) solution in the presence of tetraoctylammonium (TOA) countercations (see the Experimental Section for details). After the reaction, the synthesized product was washed by a solvent to remove excess reagents.

The final purified product dissolved in DCM shows well-defined peaks at 667 and 504 nm in its UV−vis absorption spectrum (Figure S2), which is completely different from that of $[Ag_{29}(1,3\text{-BDT})_{12}]^{3-}$ NC,[42] whose prominent absorption peak appears at 440 nm. The absence of the surface-plasmon-resonance peak for Ag nanoparticles and the presence of multiple peaks suggest the formation of a new cluster size with 1,2-BDT. The purified NC product in a dimethylformamide solution was layered with ethanol (see the Experimental Section for details) to obtain single crystals in order to determine the chemical formula, electronic charge, and molecular structure of the NC.

Electrospray ionization mass spectrometry (ESI-MS) of a single-crystal solution of the NCs showed a prominent peak at m/z 604 in negative-ion mode (Figure 1a). Expansion of this peak revealed a characteristic Ag isotopic pattern with a peak separation of m/z 0.33 (inset of Figure 1a), suggesting the charge of the molecular ion to be 3−. Considering Ag and BDT, the total mass of this ion for the m/z 604 peak (i.e., $604 \times 3 = 1812$) was assigned to a composition of $[Ag_9(1,2\text{-BDT})_6]^{3-}$. This assigned composition was further confirmed by comparing a simulated mass spectrum for $[Ag_9(1,2\text{-BDT})_6]^{3-}$ with that of the experiment, wherein they matched

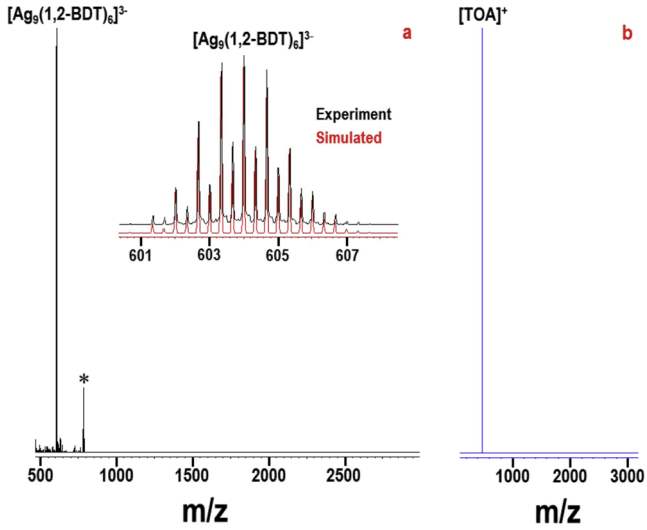

Figure 1. ESI-MS of $[Ag_9(1,2\text{-BDT})_6]^{3-}$ NCs in (a) negative-ion and (b) positive-ion modes. Inset of part a: Comparison of a simulated mass spectrum for $[Ag_9(1,2\text{-BDT})_6]^{3-}$ with the experiment. The asterisk peak in part a is due to the fragment $[Ag_8(1,2\text{-BDT})_5]^{2-}$, originating from its parent cluster $[Ag_9(1,2\text{-BDT})_6]^{3-}$.

perfectly (inset of Figure 1a). Along with the prominent $[Ag_9(1,2\text{-BDT})_6]^{3-}$ peak, a minor peak for $[Ag_8(1,2\text{-BDT})_5]^{2-}$ was also observed (denoted with an asterisk in Figure 1a), originating from $[Ag_9(1,2\text{-BDT})_6]^{3-}$ by the loss of one [Ag(1,2-BDT)] unit, which is a common occurrence in ESI-MS of Ag NCs.[43] The positive-ion-mode ESI-MS (Figure 1b) showed a single peak for $[TOA]^+$, indicating stabilization of the $[Ag_9(1,2\text{-BDT})_6]^{3-}$ clusters with counterions of $[TOA]^+$.

Analysis of the collected single-crystal X-ray diffraction data further validated the overall composition of the NCs that was deduced from ESI-MS. The $[Ag_9(1,2\text{-BDT})_6]^{3-}$ NCs crystallized in the monoclinic space group $P2_1/c$ (Table S1). Its unit cell and the packing of NCs are shown in Figure S3, revealing three TOA^+ ions per cluster, confirming the 3− charge state of the Ag_9 cluster.

The structure of a single nonanuclear Ag cluster is shown in Figure 2a. The asymmetric unit contains the halves of the Ag nonanuclear clusters. Both halves adopt the shape of two deformed square pyramids sharing one Ag atom. Hence, the shared Ag atom appears at the center of the cluster surrounded by eight Ag corner atoms (Figure 2b). Distances between the central Ag atom and each of the remaining eight are in the ranges of 3.096(1)−3.292(1) and 3.0322(9)−

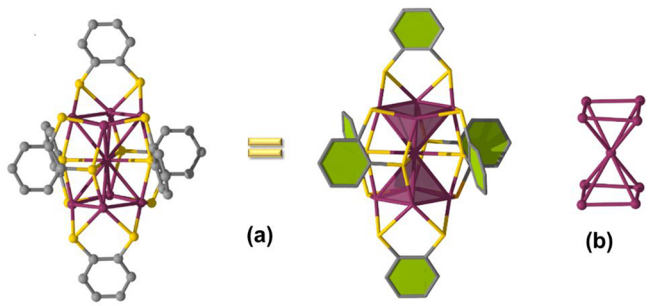

Figure 2. Crystal structure of the Ag_9 NC: (a) whole $[Ag_9(1,2\text{-BDT})_6]^{3-}$ anion; (b) Ag_9 metal skeleton of the $[Ag_9(1,2\text{-BDT})_6]^{3-}$ cluster. Color legends: gray, C; plum, Ag; yellow, S.

https://doi.org/10.1021/acs.inorgchem.1c00334
Inorg. Chem. 2021, 60, 4306−4312

3.3232(9) Å in the cases of clusters I and II, respectively (Figure S4). Therefore, the Ag−Ag distances in the $[Ag_9(BDT)_6]^{3-}$ anions are definitely longer than the Ag−Ag distance of 2.88 Å in bulk Ag, indicating weak interactions among the Ag atoms. Each cluster is capped by six bidentate thiolate ligands, with two in the apical positions and four in the equatorial plane coordinated in two different connectivity modes: μ_3-η^1:η^2:η^1 and μ_4-η^1:η^2:η^1:η^1, respectively. There are eight μ_2-S atoms bonded to the square base of each pyramid to form Ag_9S_8 and four μ_3-S atoms shared in the center and connected to the top and bottom Ag atoms of the Ag_9 core to give the final framework of a rod-shaped $Ag_9(SR)_{12}$ cluster (Figure 3). The packing structure of the crystal clearly reveals

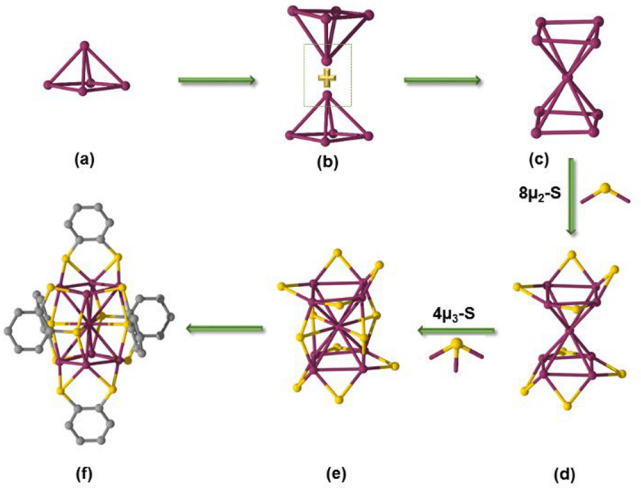

Figure 3. Construction of the $[Ag_9(1,2\text{-}BDT)_6]^{3-}$ NC. (a) Ag_5 of the square-pyramidal building block. (b) Linear assembly of two square pyramids through pyramidal vertex sharing to form the Ag_9 skeleton structure as shown in part c. (d) Formation of the Ag_9S_8 framework upon bridging of the eight edges with eight μ_2-S atoms of the 1,2-BDT ligands. (e) Bridging of Ag_9S_8 with four μ_3-S atoms of the 1,2-BDT ligands to form a rod-shaped Ag_9S_{12} unit. The C atoms of ligands are omitted in parts d and e for clarity. (f) Total structure of the NC. Color legends: gray, C; plum, Ag; yellow, S.

the location of the counterions, $[TOA]^+$ between the $[Ag_9(1,2\text{-}BDT)_6]^{3-}$ anions, thus balancing the overall charge of the crystal, and the clusters of the same type are located at the same coordinate *x*, forming the 2D layers in the structure parallel to the plane (011) (Figure S3). An overlay of the two crystallographically independent clusters reveals their similarity (Figure S4). Thus, the root-mean-square deviation for the overlay equals 0.1444 Å, and the maximum distance between two equivalent atoms in the overlay (Max. D) is 0.2995 Å (excluding H atoms). The formation of a Ag_9 skeleton can also be viewed as the simultaneous interaction of two Ag_4 squares and a single Ag atom, as shown in Figure S5. Upon capping of this Ag_9 metal unit with six 1,2-BDT ligands, the total structure of $[Ag_9(1,2\text{-}BDT)_6]^{3-}$ is obtained.

The photophysical properties of $[Ag_9(1,2\text{-}BDT)_6]^{3-}$ NCs were further studied using time-resolved photoluminescence (PL) and femtosecond transient absorption (fs-TA) spectroscopies (see the Supporting Information for details). This cluster shows a broad PL peak in the near-IR region with a maximum intensity at ~820 nm (excitation = 480 nm; Figure S6A). This emission may be originating from the direct electron−hole recombination. The PL excitation spectrum (Figure S6B) for emission at 820 nm is found to be similar to the absorption spectrum, suggesting that PL is emanating from the NC's core. Moreover, the PL emission and excitation maps indicated that this emission is arising from a single species, i.e., $[Ag_9(1,2\text{-}BDT)_6]^{3-}$ (Figure S6C). Notably, the emission peak position of the larger-sized $[Ag_{29}(1,3\text{-}BDT)_{12}]^{3-}$ cluster is 659 nm, which is higher in energy compared to that of $[Ag_9(1,2\text{-}BDT)_6(TPP)_4]^{3-}$ (820 nm).[42] This suggests that PL of the NCs in this size regime is largely electronic-structure-dependent rather than being dominated by quantum size effects. It should be noted that the time-resolved PL data (Figure S7) show an average lifetime of 1.43 ns. This ultrafast excited-state relaxation is further supported by fs-TA spectroscopy, which shows two excited-state decay constants of 59 ps (42%) and 1.5 ns (58%) (Figure S8). The fast component could be attributed to the carrier recombination, which is likely assisted by surface trap states.

COMPUTATIONAL MODELING

Time-dependent DFT (TDDFT) was used to theoretically investigate the optical and electronic transitions in the $[Ag_9(1,2\text{-}BDT)_6]^{3-}$ NC. The geometry of the NCs was optimized with the Tao, Perdew, Staroverov, and Scuseria[44,45] exchange-correlation function augmented with Grimme D3 corrections,[46] as implemented in the *ADF* software. Relativistic effects were treated using the zeroth-order regular approximation, and the COSMO implicit solvent model[47−49] was employed to describe the solvent effect. Thereafter, the optical absorption properties of this cluster were calculated using TDDFT with the same setup. A Lorentzian broadening of 0.1 eV was applied to TDDFT excitation energies to generate the spectrum. There was less than a 0.1 eV difference between the peak positions in the calculated and experimental spectra.

Our TDDFT modeling reasonably reproduced the main peaks and shoulders observed in the experimental spectrum (Figure 4). We further projected the main transition features onto the molecular orbitals (Figure 5), which show the large contribution of the ligands to the electronic structure due to the small cluster size. The highest occupied molecular orbitals (HOMOs) of the cluster have contributions from both the p

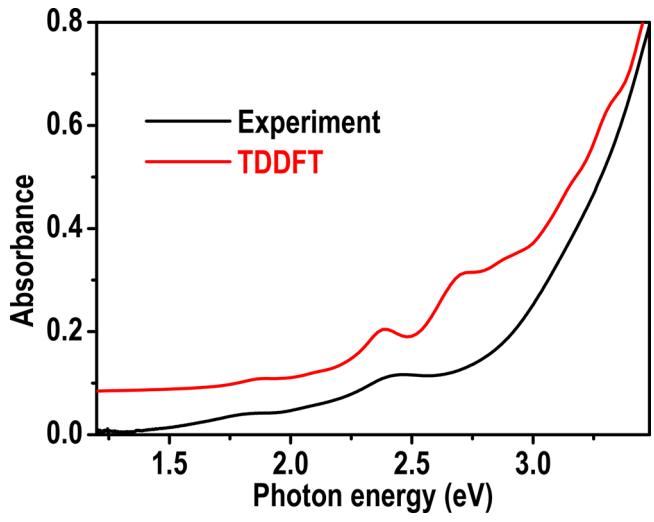

Figure 4. Experimental (black curve) and simulated (red curve) UV−vis absorption spectra of the $[Ag_9(1,2\text{-}BDT)_6]^{3-}$ NCs.

https://doi.org/10.1021/acs.inorgchem.1c00334
Inorg. Chem. 2021, 60, 4306−4312

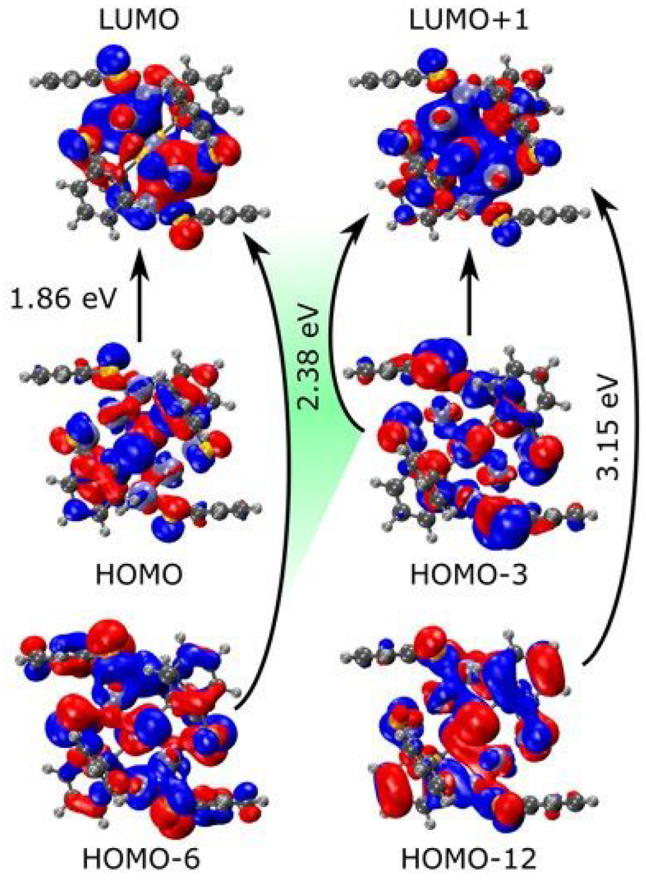

Figure 5. Molecular orbitals with the highest contributions to the important transitions of $[Ag_9(1,2\text{-BDT})_6]^{3-}$ NCs at ~1.9 and ~2.4 eV.

system of the ligands and the d orbitals of the Ag atoms. Whereas the lowest unoccupied molecular orbital (LUMO) resembles a p-shaped superatomic orbital centered on the Ag core of the cluster, other unoccupied orbitals have more complex shapes that cannot be easily assigned to any specific type. The experimental peak at 1.86 eV (667 nm) corresponds to the calculated peak at 1.9 eV, which is essentially HOMO-to-LUMO excitation (99%). The second experimental feature at 2.46 eV (504 nm) corresponds to the simulated peak at 2.39 eV, which comes mainly from the HOMO−6-to-LUMO +1 excitation (69%). The main absorption area is a combination of several transitions, like the ones observed at 3.15 and 3.49 eV. Table S2 and Figure S9 provide more details on the orbital contributions to important optical transitions. The molar absorption coefficients of $[Ag_9(1,2\text{-BDT})_6](TOA)_3$ NC are found to be ~0.4×10^4 and ~0.11×10^4 $M^{-1}cm^{-1}$ for the absorption peaks at 504 and 667 nm, respectively, in DCM. In the solid state (as powder), this cluster is stable in air for approximately 2 weeks, while in solution (in DCM), the cluster is stable for ~24 h (Figure S10). The partial degradation product of the cluster that forms over time in solution seems to be a result of dissolution because we found no evidence of new cluster types forming (i.e., $[Ag_9(1,2\text{-BDT})_6](TOA)_3$ was the only cluster species observed).

CONCLUSION

In conclusion, we developed an approach to synthesize few-atom ($n < 10$) stable Ag NCs. $[Ag_9(1,2\text{-BDT})_6]^{3-}$ is the smallest crystallized Ag NC, with just a single metallically bonded Ag atom at its center. The specific distribution of bidentate thiol ligands on the surface tailors the cluster skeleton into an elongated body-centered cage. The crystal structure shows that the metal core is a combination of two square pyramids that share one vertex capped by six small-footprint dithiolate ligands. Theoretical calculations show that the simulated optical transitions are in good agreement with the experimental optical absorption spectra. These findings pave the way for the development of atomically precise metal NCs with single-digit metallic cores and stimulate research into their catalytic applications.

EXPERIMENTAL SECTION

Chemicals. All chemicals, including silver nitrate ($AgNO_3$, 99%), 1,2-benzenedithiol (1,2-BDT), sodium borohydride ($NaBH_4$, 99.99% metals basis), and tetraoctylammonium bromide (TOAB), were purchased from Sigma-Aldrich and used without further purification. Solvents, including methanol, dichloromethane (DCM), dimethylformamide (DMF), and acetonitrile, were used from Sigma as received. Distilled water (H_2O) was obtained from Milli-Q (Millipore apparatus).

Synthesis and Crystallization of the $[Ag_9(1,2\text{-BDT})_6](TOA)_3$ NC. This NC was prepared by dissolving $AgNO_3$ (20 mg, 0.117 mmol) in methanol. Then, a solution of the 1,2-BDT (13.5 μL, 0.117 mmol) ligand in 10 mL of DCM was added to form a yellow turbid complex, indicating formation of the Ag−S bonds. The reaction mixture was reduced using a fresh aqueous solution of $NaBH_4$ (20 mg, 0.5 mmol) in the presence of TOAB (0.4115 mg), resulting in a dark-brown solution that was left under continuous stirring for 90 min at room temperature. To purify the synthesized cluster, we centrifuged the solution at 9500 rpm; the product consisted of a dark-brown precipitate that was neglected, and the dark-brown supernatant was dried under vacuum and washed several times with excess methanol to remove byproducts. The purified NC product (5 mg) was dissolved in DMF (2 mL) and filtered using a syringe filter. The cluster solution was layered with ethanol at 5 °C, forming single crystals (within 1 week) suitable for X-ray crystallography.

ASSOCIATED CONTENT

Supporting Information

The Supporting Information is available free of charge at https://pubs.acs.org/doi/10.1021/acs.inorgchem.1c00334.

Details of characterization, crystallographic data, and DFT results (PDF)

Accession Codes

CCDC 2045979 contains the supplementary crystallographic data for this paper. These data can be obtained free of charge via www.ccdc.cam.ac.uk/data_request/cif, or by emailing data_request@ccdc.cam.ac.uk, or by contacting The Cambridge Crystallographic Data Centre, 12 Union Road, Cambridge CB2 1EZ, UK; fax: +44 1223 336033.

AUTHOR INFORMATION

Corresponding Author

Osman M. Bakr − *Division of Physical Sciences and Engineering, King Abdullah University of Science and Technology (KAUST), Thuwal 23955-6900, Saudi Arabia; KAUST Catalysis Center, Division of Physical Sciences and Engineering, King Abdullah University of Science and Technology (KAUST), Thuwal 23955-6900, Saudi Arabia;*

https://doi.org/10.1021/acs.inorgchem.1c00334
Inorg. Chem. 2021, 60, 4306−4312

orcid.org/0000-0002-3428-1002; Email: osman.bakr@kaust.edu.sa

Authors

Badriah J. Alamer − *Division of Physical Sciences and Engineering, King Abdullah University of Science and Technology (KAUST), Thuwal 23955-6900, Saudi Arabia; KAUST Catalysis Center, Division of Physical Sciences and Engineering, King Abdullah University of Science and Technology (KAUST), Thuwal 23955-6900, Saudi Arabia; Department of Chemistry, College of Sciences, Taif University, Taif 11099, Saudi Arabia*

Megalamane S. Bootharaju − *Center for Nanoparticle Research, Institute for Basic Science, Seoul 08826, Republic of Korea; School of Chemical and Biological Engineering and Institute of Chemical Processes, Seoul National University, Seoul 08826, Republic of Korea*

Sergey M. Kozlov − *Department of Chemical and Biomolecular Engineering, Faculty of Engineering, National University of Singapore, Singapore 119260, Singapore*

Zhen Cao − *Division of Physical Sciences and Engineering, King Abdullah University of Science and Technology (KAUST), Thuwal 23955-6900, Saudi Arabia; KAUST Catalysis Center, Division of Physical Sciences and Engineering, King Abdullah University of Science and Technology (KAUST), Thuwal 23955-6900, Saudi Arabia*

Aleksander Shkurenko − *Division of Physical Sciences and Engineering, King Abdullah University of Science and Technology (KAUST), Thuwal 23955-6900, Saudi Arabia; Functional Materials Design, Discovery and Development Research Group, Advanced Membranes and Porous Materials Center, King Abdullah University of Science and Technology (KAUST), Thuwal 23955-6900, Saudi Arabia;* orcid.org/0000-0001-7136-2277

Saidkhodzha Nematulloev − *Division of Physical Sciences and Engineering, King Abdullah University of Science and Technology (KAUST), Thuwal 23955-6900, Saudi Arabia; Functional Materials Design, Discovery and Development Research Group, Advanced Membranes and Porous Materials Center, King Abdullah University of Science and Technology (KAUST), Thuwal 23955-6900, Saudi Arabia*

Partha Maity − *Advanced Membranes and Porous Materials Center, Division of Physical Sciences and Engineering, King Abdullah University of Science and Technology (KAUST), Thuwal 23955-6900, Saudi Arabia; KAUST Catalysis Center, Division of Physical Sciences and Engineering, King Abdullah University of Science and Technology (KAUST), Thuwal 23955-6900, Saudi Arabia; Division of Physical Sciences and Engineering, King Abdullah University of Science and Technology (KAUST), Thuwal 23955-6900, Saudi Arabia;* orcid.org/0000-0002-0293-7118

Omar F. Mohammed − *Advanced Membranes and Porous Materials Center, Division of Physical Sciences and Engineering, King Abdullah University of Science and Technology (KAUST), Thuwal 23955-6900, Saudi Arabia; KAUST Catalysis Center, Division of Physical Sciences and Engineering, King Abdullah University of Science and Technology (KAUST), Thuwal 23955-6900, Saudi Arabia; Division of Physical Sciences and Engineering, King Abdullah University of Science and Technology (KAUST), Thuwal 23955-6900, Saudi Arabia;* orcid.org/0000-0001-8500-1130

Mohamed Eddaoudi − *Division of Physical Sciences and Engineering, King Abdullah University of Science and Technology (KAUST), Thuwal 23955-6900, Saudi Arabia; Functional Materials Design, Discovery and Development Research Group, Advanced Membranes and Porous Materials Center, King Abdullah University of Science and Technology (KAUST), Thuwal 23955-6900, Saudi Arabia;* orcid.org/0000-0003-1916-9837

Luigi Cavallo − *Division of Physical Sciences and Engineering, King Abdullah University of Science and Technology (KAUST), Thuwal 23955-6900, Saudi Arabia; KAUST Catalysis Center, Division of Physical Sciences and Engineering, King Abdullah University of Science and Technology (KAUST), Thuwal 23955-6900, Saudi Arabia;* orcid.org/0000-0002-1398-338X

Jean-Marie Basset − *Division of Physical Sciences and Engineering, King Abdullah University of Science and Technology (KAUST), Thuwal 23955-6900, Saudi Arabia; KAUST Catalysis Center, Division of Physical Sciences and Engineering, King Abdullah University of Science and Technology (KAUST), Thuwal 23955-6900, Saudi Arabia;* orcid.org/0000-0003-3166-8882

Complete contact information is available at: https://pubs.acs.org/10.1021/acs.inorgchem.1c00334

Notes

The authors declare no competing financial interest.

■ ACKNOWLEDGMENTS

This work was supported by KAUST. Computational time was afforded by the resources of the Supercomputing Laboratory at KAUST in Thuwal, Saudi Arabia.

■ REFERENCES

(1) Xie, Y.-P.; Shen, Y.-L.; Duan, G.-X.; Han, J.; Zhang, L.-P.; Lu, X. Silver nanoclusters: synthesis, structures and photoluminescence. *Mater. Chem. Front.* **2020**, *4* (8), 2205−2222.

(2) Jin, R. Atomically precise metal nanoclusters: stable sizes and optical properties. *Nanoscale* **2015**, *7* (5), 1549−1565.

(3) Joshi, C. P.; Bootharaju, M. S.; Bakr, O. M. Tuning Properties in Silver Clusters. *J. Phys. Chem. Lett.* **2015**, *6* (15), 3023−3035.

(4) Lu, Y.; Chen, W. Sub-nanometre sized metal clusters: from synthetic challenges to the unique property discoveries. *Chem. Soc. Rev.* **2012**, *41* (9), 3594−3623.

(5) Giljohann, D. A.; Seferos, D. S.; Daniel, W. L.; Massich, M. D.; Patel, P. C.; Mirkin, C. A. Gold Nanoparticles for Biology and Medicine. *Angew. Chem., Int. Ed.* **2010**, *49* (19), 3280−3294.

(6) Han, G.; Ghosh, P.; Rotello, V. M. Functionalized gold nanoparticles for drug delivery. *Nanomedicine* **2007**, *2* (1), 113−123.

(7) Mathew, A.; Pradeep, T. Noble Metal Clusters: Applications in Energy, Environment, and Biology. *Part. Part. Syst. Charact.* **2014**, *31* (10), 1017−1053.

(8) Peng, M.; Na, N.; Ouyang, J. A Fluorescence Light-Up Silver Nanocluster Beacon Modulated by Metal Ions and Its Application in Telomerase-Activity Detection. *Chem. - Eur. J.* **2019**, *25* (14), 3598−3605.

(9) Tsunoyama, H.; Liu, Y.; Akita, T.; Ichikuni, N.; Sakurai, H.; Xie, S.; Tsukuda, T. Size-Controlled Synthesis of Gold Clusters as Efficient Catalysts for Aerobic Oxidation. *Catal. Surv. Asia* **2011**, *15* (4), 230−239.

(10) Urushizaki, M.; Kitazawa, H.; Takano, S.; Takahata, R.; Yamazoe, S.; Tsukuda, T. Synthesis and Catalytic Application of Ag_{44} Clusters Supported on Mesoporous Carbon. *J. Phys. Chem. C* **2015**, *119* (49), 27483−27488.

(11) Wang, Y.; Wan, X.-K.; Ren, L.; Su, H.; Li, G.; Malola, S.; Lin, S.; Tang, Z.; Häkkinen, H.; Teo, B. K.; Wang, Q.-M.; Zheng, N. Atomically Precise Alkynyl-Protected Metal Nanoclusters as a Model Catalyst: Observation of Promoting Effect of Surface Ligands on Catalysis by Metal Nanoparticles. *J. Am. Chem. Soc.* **2016**, *138* (10), 3278−3281.
(12) Tyo, E. C.; Vajda, S. Catalysis by clusters with precise numbers of atoms. *Nat. Nanotechnol.* **2015**, *10*, 577.
(13) Yang, X.-F.; Wang, A.; Qiao, B.; Li, J.; Liu, J.; Zhang, T. Single-Atom Catalysts: A New Frontier in Heterogeneous Catalysis. *Acc. Chem. Res.* **2013**, *46* (8), 1740−1748.
(14) Lu, Y.; Chen, W. Size effect of silver nanoclusters on their catalytic activity for oxygen electro-reduction. *J. Power Sources* **2012**, *197*, 107−110.
(15) Herzing, A. A.; Kiely, C. J.; Carley, A. F.; Landon, P.; Hutchings, G. J. Identification of Active Gold Nanoclusters on Iron Oxide Supports for CO Oxidation. *Science* **2008**, *321* (5894), 1331−1335.
(16) Kappes, M. M.; Radi, P.; Schär, M.; Schumacher, E. Probes for electronic and geometrical shell structure effects in alkali-metal clusters. Photoionization measurements on K_xLi, K_xMg and K_xZn ($x < 25$). *Chem. Phys. Lett.* **1985**, *119* (1), 11−16.
(17) Yang, H.; Wang, Y.; Huang, H.; Gell, L.; Lehtovaara, L.; Malola, S.; Häkkinen, H.; Zheng, N. All-thiol-stabilized Ag_{44} and $Au_{12}Ag_{32}$ nanoparticles with single-crystal structures. *Nat. Commun.* **2013**, *4*, 2422.
(18) Joshi, C. P.; Bootharaju, M. S.; Alhilaly, M. J.; Bakr, O. M. $[Ag_{25}(SR)_{18}]^-$: The "Golden" Silver Nanoparticle. *J. Am. Chem. Soc.* **2015**, *137* (36), 11578−11581.
(19) Wang, Z.; Su, H.-F.; Tan, Y.-Z.; Schein, S.; Lin, S.-C.; Liu, W.; Wang, S.-A.; Wang, W.-G.; Tung, C.-H.; Sun, D.; Zheng, L.-S. Assembly of silver Trigons into a buckyball-like Ag_{180} nanocage. *Proc. Natl. Acad. Sci. U. S. A.* **2017**, *114* (46), 12132−12137.
(20) Bian, S.-D.; Jia, J.-H.; Wang, Q.-M. High-Nuclearity Silver Clusters Templated by Carbonates Generated from Atmospheric Carbon Dioxide Fixation. *J. Am. Chem. Soc.* **2009**, *131* (10), 3422−3423.
(21) Dhayal, R. S.; Liao, J. H.; Liu, Y. C.; Chiang, M. H.; Kahlal, S.; Saillard, J. Y.; Liu, C. W. $[Ag_{21}\{S_2P(OiPr)_2\}_{12}]^+$: An Eight-Electron Superatom. *Angew. Chem., Int. Ed.* **2015**, *54* (12), 3702−3706.
(22) Ahmar, S.; MacDonald, D. G.; Vijayaratnam, N.; Battista, T. L.; Workentin, M. S.; Corrigan, J. F. A Nanoscopic 3D Polyferrocenyl Assembly: The Triacontakaihexa(ferrocenylmethylthiolate) $[Ag_{48}(\mu_4\text{-}S)6(\mu_2/3\text{-}SCH_2Fc)_{36}]$. *Angew. Chem., Int. Ed.* **2010**, *49* (26), 4422−4424.
(23) Li, G.; Lei, Z.; Wang, Q.-M. Luminescent Molecular Ag−S Nanocluster $[Ag_{62}S_{13}(SBut)_{32}](BF_4)_4$. *J. Am. Chem. Soc.* **2010**, *132* (50), 17678−17679.
(24) Chen, Z.-Y.; Tam, D. Y. S.; Mak, T. C. W. Ethynide-stabilized high-nuclearity silver(i) sulfido molecular clusters assembled using organic sulfide precursors. *Chem. Commun.* **2016**, *52* (36), 6119−6122.
(25) Fenske, D.; Persau, C.; Dehnen, S.; Anson, C. E. Syntheses and Crystal Structures of the Ag-S Cluster Compounds $[Ag_{70}S_{20}(SPh)_{28}(dppm)_{10}](CF_3CO_2)_2$ and $[Ag_{262}S_{100}(StBu)_{62}(dppb)_6]$. *Angew. Chem., Int. Ed.* **2004**, *43* (3), 305−309.
(26) Liu, J.-W.; Feng, L.; Su, H.-F.; Wang, Z.; Zhao, Q.-Q.; Wang, X.-P.; Tung, C.-H.; Sun, D.; Zheng, L.-S. Anisotropic Assembly of Ag_{52} and Ag_{76} Nanoclusters. *J. Am. Chem. Soc.* **2018**, *140* (5), 1600−1603.
(27) Huang, R.-W.; Xu, Q.-Q.; Lu, H.-L.; Guo, X.-K.; Zang, S.-Q.; Gao, G.-G.; Tang, M.-S.; Mak, T. C. W. Self-assembly of an unprecedented polyoxomolybdate anion $[Mo_{20}O_{66}]^{12-}$ in a giant peanut-like 62-core silver-thiolate nanocluster. *Nanoscale* **2015**, *7* (16), 7151−7154.
(28) Bootharaju, M. S.; Kozlov, S. M.; Cao, Z.; Harb, M.; Maity, N.; Shkurenko, A.; Parida, M. R.; Hedhili, M. N.; Eddaoudi, M.; Mohammed, O. F.; Bakr, O. M.; Cavallo, L.; Basset, J.-M. Doping-Induced Anisotropic Self-Assembly of Silver Icosahedra in $[Pt_2Ag_{23}C_{l7}(PPh_3)_{10}]$ Nanoclusters. *J. Am. Chem. Soc.* **2017**, *139* (3), 1053−1056.
(29) Alhilaly, M. J.; Bootharaju, M. S.; Joshi, C. P.; Besong, T. M.; Emwas, A.-H.; Juarez-Mosqueda, R.; Kaappa, S.; Malola, S.; Adil, K.; Shkurenko, A.; Häkkinen, H.; Eddaoudi, M.; Bakr, O. M. $[Ag_{67}(SPhMe_2)_{32}(PPh_3)_8]^{3+}$: Synthesis, Total Structure, and Optical Properties of a Large Box-Shaped Silver Nanocluster. *J. Am. Chem. Soc.* **2016**, *138* (44), 14727−14732.
(30) Wu, Z.; Lanni, E.; Chen, W.; Bier, M. E.; Ly, D.; Jin, R. High Yield, Large Scale Synthesis of Thiolate-Protected Ag_7 Clusters. *J. Am. Chem. Soc.* **2009**, *131* (46), 16672−16674.
(31) Udaya Bhaskara Rao, T.; Pradeep, T. Luminescent Ag_7 and Ag_8 Clusters by Interfacial Synthesis. *Angew. Chem., Int. Ed.* **2010**, *49* (23), 3925−3929.
(32) Rao, T. U. B.; Nataraju, B.; Pradeep, T. Ag_9 Quantum Cluster through a Solid-State Route. *J. Am. Chem. Soc.* **2010**, *132* (46), 16304−16307.
(33) Ren, X.; Fu, J.; Lin, X.; Fu, X.; Yan, J.; Wu, R. a.; Liu, C.; Huang, J. Cluster-to-cluster transformation among Au_6, Au_8 and Au_{11} nanoclusters. *Dalton Trans.* **2018**, *47* (22), 7487−7491.
(34) Konishi, K.; Iwasaki, M.; Shichibu, Y. Phosphine-Ligated Gold Clusters with Core+exo Geometries: Unique Properties and Interactions at the Ligand−Cluster Interface. *Acc. Chem. Res.* **2018**, *51* (12), 3125−3133.
(35) Jiang, D.-e.; Overbury, S. H.; Dai, S. Structure of $Au_{15}(SR)_{13}$ and Its Implication for the Origin of the Nucleus in Thiolated Gold Nanoclusters. *J. Am. Chem. Soc.* **2013**, *135* (24), 8786−8789.
(36) Gao, X.; He, S.; Zhang, C.; Du, C.; Chen, X.; Xing, W.; Chen, S.; Clayborne, A.; Chen, W. Single Crystal Sub-Nanometer Sized $Cu_6(SR)_6$ Clusters: Structure, Photophysical Properties, and Electrochemical Sensing. *Adv. Sci.* **2016**, *3* (12), 1600126.
(37) Chen, Y.; Zeng, C.; Liu, C.; Kirschbaum, K.; Gayathri, C.; Gil, R. R.; Rosi, N. L.; Jin, R. Crystal Structure of Barrel-Shaped Chiral $Au_{130}(p\text{-}MBT)_{50}$ Nanocluster. *J. Am. Chem. Soc.* **2015**, *137* (32), 10076−10079.
(38) Chen, Y.; Liu, C.; Tang, Q.; Zeng, C.; Higaki, T.; Das, A.; Jiang, D.-e.; Rosi, N. L.; Jin, R. Isomerism in $Au_{28}(SR)_{20}$ Nanocluster and Stable Structures. *J. Am. Chem. Soc.* **2016**, *138* (5), 1482−1485.
(39) Zheng, K.; Yuan, X.; Xie, J. Effect of ligand structure on the size control of mono- and bi-thiolate-protected silver nanoclusters. *Chem. Commun.* **2017**, *53* (70), 9697−9700.
(40) Yuan, X.; Goswami, N.; Chen, W.; Yao, Q.; Xie, J. Insights into the effect of surface ligands on the optical properties of thiolated Au_{25} nanoclusters. *Chem. Commun.* **2016**, *52* (30), 5234−5237.
(41) Krommenhoek, P. J.; Wang, J.; Hentz, N.; Johnston-Peck, A. C.; Kozek, K. A.; Kalyuzhny, G.; Tracy, J. B. Bulky Adamantanethiolate and Cyclohexanethiolate Ligands Favor Smaller Gold Nanoparticles with Altered Discrete Sizes. *ACS Nano* **2012**, *6* (6), 4903−4911.
(42) AbdulHalim, L. G.; Bootharaju, M. S.; Tang, Q.; Del Gobbo, S.; AbdulHalim, R. G.; Eddaoudi, M.; Jiang, D.-e.; Bakr, O. M. $Ag_{29}(BDT)_{12}(TPP)_4$: A Tetravalent Nanocluster. *J. Am. Chem. Soc.* **2015**, *137* (37), 11970−11975.
(43) Desireddy, A.; Conn, B. E.; Guo, J.; Yoon, B.; Barnett, R. N.; Monahan, B. M.; Kirschbaum, K.; Griffith, W. P.; Whetten, R. L.; Landman, U.; Bigioni, T. P. Ultrastable silver nanoparticles. *Nature* **2013**, *501* (7467), 399−402.
(44) Tao, J.; Perdew, J. P.; Staroverov, V. N.; Scuseria, G. E. Climbing the Density Functional Ladder: Nonempirical Meta-Generalized Gradient Approximation Designed for Molecules and Solids. *Phys. Rev. Lett.* **2003**, *91* (14), 146401.
(45) Staroverov, V. N.; Scuseria, G. E.; Tao, J.; Perdew, J. P. Comparative assessment of a new nonempirical density functional: Molecules and hydrogen-bonded complexes. *J. Chem. Phys.* **2003**, *119* (23), 12129−12137.
(46) Grimme, S.; Ehrlich, S.; Goerigk, L. Effect of the damping function in dispersion corrected density functional theory. *J. Comput. Chem.* **2011**, *32* (7), 1456−1465.

https://doi.org/10.1021/acs.inorgchem.1c00334
Inorg. Chem. 2021, 60, 4306−4312

(47) Klamt, A.; Schuurmann, G. COSMO: a new approach to dielectric screening in solvents with explicit expressions for the screening energy and its gradient. *J. Chem. Soc., Perkin Trans. 2* **1993**, No. 5, 799−805.
(48) Klamt, A. Conductor-like Screening Model for Real Solvents: A New Approach to the Quantitative Calculation of Solvation Phenomena. *J. Phys. Chem.* **1995**, *99* (7), 2224−2235.
(49) Klamt, A.; Jonas, V. Treatment of the outlying charge in continuum solvation models. *J. Chem. Phys.* **1996**, *105* (22), 9972−9981.

https://doi.org/10.1021/acs.inorgchem.1c00334
Inorg. Chem. 2021, 60, 4306−4312